

# Faraday Discussions

Accepted Manuscript



This manuscript will be presented and discussed at a forthcoming Faraday Discussion meeting. All delegates can contribute to the discussion which will be included in the final volume.

**Register now to attend!** Full details of all upcoming meetings: <http://rsc.li/fd-upcoming-meetings>



This is an *Accepted Manuscript*, which has been through the Royal Society of Chemistry peer review process and has been accepted for publication.

*Accepted Manuscripts* are published online shortly after acceptance, before technical editing, formatting and proof reading. Using this free service, authors can make their results available to the community, in citable form, before we publish the edited article. We will replace this *Accepted Manuscript* with the edited and formatted *Advance Article* as soon as it is available.

You can find more information about *Accepted Manuscripts* in the [Information for Authors](#).

Please note that technical editing may introduce minor changes to the text and/or graphics, which may alter content. The journal's standard [Terms & Conditions](#) and the [Ethical guidelines](#) still apply. In no event shall the Royal Society of Chemistry be held responsible for any errors or omissions in this *Accepted Manuscript* or any consequences arising from the use of any information it contains.

## In Situ TEM Study of Li-Au Reaction in an Electrochemical Liquid Cell

Zhiyuan Zeng,<sup>1</sup> Wen-I Liang<sup>1,2</sup>, Ying-Hao Chu<sup>2</sup>, Haimei Zheng<sup>1,3\*</sup>

<sup>1</sup>*Materials Sciences Division, Lawrence Berkeley National Laboratory, Berkeley, CA 94720, USA*

<sup>2</sup>*Department of Materials Science and Engineering, National Chiao Tung University, Hsinchu, 30010, Taiwan*

<sup>3</sup>*Department of Materials Science and Engineering, University of California, Berkeley, California 94720, United States*

\*Correspondence should be addressed to: [hmzheng@lbl.gov](mailto:hmzheng@lbl.gov)

### Abstract

We study lithiation of Au electrode in an electrochemical liquid cell using transmission electron microscopy (TEM). The commercial liquid electrolyte for lithium ion batteries (1M lithium hexafluorophosphate LiPF<sub>6</sub> dissolved in 1:1 (v/v) ethylene carbonate (EC) and diethyl carbonate (DEC)) was used. Three distinct types of morphology changes during reaction, including gradual dissolution, explosive reaction and local expansion/shrinkage, are observed. It is expected that significant stress is generated from lattice expansion during lithium-gold alloy formation. There is vigorous bubble formation from electrolyte decomposition likely due to the catalytic effect of Au, while the bubble generation is less severe with titanium electrodes. There is an increase of current in response to electron beam irradiation and the electron beam effects on the observed electrochemical reaction are discussed.

**Keywords:** Li-Au reaction, bubble formation, Liquid cell TEM, Electrochemical liquid

cell.

## Introduction

In commercial lithium-ion batteries, the most commonly used anode materials are graphitic carbon or other carbonaceous materials since such materials are cheap, with a good cycle-ability and the working voltage is low<sup>1,2</sup> However, the theoretical capacity of carbon electrode is only 372 mAh g<sup>-1</sup>. To decrease the reduction of cell voltage and thereby increase the energy density, anode materials with extremely negative potential and high capacity have been investigated. Metals or other materials including Sn, Cu, Sb and Si that can be alloyed with lithium are promising candidates due to their high theoretical capacity.<sup>3-10</sup> Gold (Au) reacts with lithium at low voltage forming several lithium-gold alloy phases including ones with a very high percentage of Li (up to Au<sub>4</sub>Li<sub>15</sub>)<sup>11</sup>. Au electrode can be used as the anode (although not cost effective) since it has a wide range of stable cell voltage and the lowest possible alloying/de-alloying potentials relative to the Li/Li<sup>+</sup> couple. It is known that any deviation from the potential of the Li/Li<sup>+</sup> couple will be at the expense of the overall cell voltage, and the net effect will be a reduction in the energy density of the battery. The major problem encountered in gold as well as other materials in the above is the large volume change from structural changes accompanied by lithiation and delithiation. The mechanical stress generated during this lithium uptake and release processes will cause pulverization and quick capacity fading,<sup>7</sup> which makes these materials not very practical for long time usage. The current strategies to overcome the pulverization of electrodes mainly focus on: reduction of the particle size, using composite materials, and an optimized binder material. However, the reaction

mechanisms of these materials with lithium are still far from being completely understood.

In situ liquid cell TEM allows imaging chemical reactions in liquids with high spatial resolution,<sup>12-19</sup> which opens the opportunity to address important questions on the electrode-electrolyte interfaces in a battery cell. We study Au electrode reaction with lithium during charging and discharging using an electrochemical liquid cell under a transmission electron microscope. In previous reports using gold as anode material for lithium ion batteries, although both ex situ and in situ study were applied and different Au-Li alloy phases have been achieved,<sup>4, 11, 20-22</sup> Au-Li reaction has never been observed directly. Recently, utilizing our newly designed electrochemical liquid TEM cells, we have captured the dynamic processes of inhomogeneous lithiation, lithium metal dendritic growth, electrolyte decomposition and solid-electrolyte interface formation.<sup>23</sup> Here, using the same electrochemical liquid cell, we captured different types of lithiation reaction of Au electrode in commercial battery electrolyte by real time imaging. The catalytic roles of Au on electrolyte decomposition and the beam effects are discussed based on control experiments or theoretical calculations.

## Experimental

The electrochemical cells were fabricated by following a similar procedure as reported previously.<sup>23</sup> We used ultra-thin silicon wafers (200  $\mu\text{m}$ , 4-inches, p-doped) purchased from Virginia Semiconductor (Fredericksburg, VA). A 25 nm thick low stress silicon nitride film was evaporated on the silicon wafer as a membrane of the viewing window. The viewing windows and two reservoirs were created by photolithographic patterning and etching with KOH solution (with water to KOH ratio of 2:1). The

dimensions of the windows are  $25\ \mu\text{m} \times 6\ \mu\text{m}$ . Two 120 nm-thick gold electrodes were deposited on the bottom chips with a face-to-face distance of 20  $\mu\text{m}$ . The bottom and top chips were bonded together with a 150 nm thick sputtered indium spacer. The commercial electrolyte for lithium ion batteries, *i.e.* 1M lithium hexafluorophosphate  $\text{LiPF}_6$  dissolved in 1:1 (v/v) ethylene carbonate (EC) and diethyl carbonate (DEC), was loaded into one of the reservoirs with a syringe. We seal the cell including the reservoirs using Cu foil and epoxy. Since the window gap is less than 150 nm, no contamination from epoxy was observed during electrochemical experiments. The dimensions of a biasing cell are  $\sim 3\ \text{mm} \times 3\ \text{mm}$  in square and  $\sim 400\ \mu\text{m}$  thick. Both of the working and counter electrodes were extended to two gold pads in two reservoirs. Gold wires were bonded onto each gold pad and they were connected to the two copper pads on the TEM holder tip, which allow an electric biased to be applied. The cells were fabricated at the Marvell Nanofabrication Laboratory of the University of California at Berkeley. The TEM holder fits a JEOL 2100 TEM operated at 200 kV. Real-time videos of the electrochemical experiments were recorded with 2  $\sim$  15 frames per second. Faster recording up to 400 frames per second was also incorporated using a high speed camera provided by Direct Electron, LP (San Diego, CA) with a model number of DE-12. The electrochemical process was controlled by an electrochemical workstation (Model 660D series made by CH Instruments) connected with the TEM holder. It was used to perform in-situ cyclic voltammetry measurement.

For ex-situ experiments, we first put a droplet of Au nanowire solution (used as purchased from Nanopartz Inc.) onto the lacey carbon Cu grids and let the Cu grids dry out so that lots of Au nanowires were attach to the carbon film. Then, the TEM grids

were immersed into the lithium electrolyte with short face-to-face distance. The two Cu grids were connected with an electrochemical working station and a cyclic voltammetry with the voltage range of 0 ~ -3 V and a scan rate 0.1 V/s were applied to the two Cu grids. The morphology changes and lithiated alloy phases were examined with great details under TEM as a comparison to the in situ results.

### Results and discussion

The scheme of how gold electrode reacts with lithium ion battery electrolyte in electrochemical liquid cell set up is shown in Figure 1. The bottom left of Figure 1 shows a real electrochemical liquid cell with Au wires bonded on the Au pads on bottom chip in the reservoir area. In the home-made TEM holder, a cell pocket is designed to fit and hold the electrochemical liquid cell. Currently, only two electrodes were used. In the future, a reference electrode can be added. When electrolyte  $\text{LiPF}_6/\text{EC}/\text{DEC}$  was loaded into one of the two reservoirs, the electrolyte flows into the cell by capillary force and a thin liquid layer (~120 nm) is formed at the observatory window and everywhere inside the cell. We apply a cyclic voltammetry and monitor the electrode-electrolyte interfaces under TEM. Dynamic Au electrode reaction with Li was captured in real time.

The phase diagram of the Au-Li binary system is shown in Figure 2.<sup>24</sup> The alloys of  $\text{Au}_5\text{Li}_4$ , AuLi,  $\text{AuLi}_3$  and  $\text{Au}_4\text{Li}_{15}$  compositions are expected to form during lithiation of gold at equilibrium conditions. However, these crystalline (Li, Au) compounds may not form directly during the electrochemical-driven alloying of Au with Li despite the fact the formation energy of crystalline (Li, Au) compounds are lower than those of corresponding amorphous phase, similar to the lithiation of Si reaction.<sup>25</sup> Recent study of lithium alloying with gold electrode conducted by in situ XRD revealed that during

electrochemical cycling of gold electrode two different crystalline Au-Li alloy phases were observed. For instance,  $\text{AuLi}_1$  was formed during charging of gold electrode. During discharging  $\text{AuLi}_1$  converted into  $\text{AuLi}_2$  and subsequently dissolved leaving an amorphous phase. Both  $\text{AuLi}_1$  and  $\text{AuLi}_2$  phases are not shown in the Au-Li phase diagram, which suggests that they are metastable.<sup>22</sup> We aim to image the detailed phases and phase transition accompany with morphology changes during Au-Li reaction. Here we report the morphology changes and reaction kinetics during lithiation of gold electrode from in situ observation. From our ex situ studies only  $\text{Au}_3\text{Li}$  phase was achieved, which is reasonable since only stable phases are expected after the reaction. Detailed study of phases and phase transition during reaction in situ is in progress and the results will be reported in a future publication.

Figure 3A-I show sequential images of the electrolyte decomposition, lithiation of gold electrode and subsequent dissolution of gold electrode during a discharge-charge cycle at the early stage. At the beginning, a sharp interface between Au electrode and  $\text{LiPF}_6/\text{EC}/\text{DEC}$  is observed indicating no reaction occurred. When the cyclic voltammetry is ramped down to -0.3 V, many bubbles are formed, which suggests gaseous products are generated from electrolyte decomposition<sup>23</sup>. In the meantime, a thin Li-Au layer is formed because of the interfacial reaction between Au electrode and lithium ion battery electrolyte. Subsequently, Au electrode reacts vigorously with the electrolyte, resulting in Au layer stripping and dissolving from the outer layer to the inner part of the electrode. The starting etching point is the corner of Au electrode, then the reaction front propagates along the diagonal direction (Figure 3C-E). A large part of the Au corner etched away within 2 s, defined as the “first round dissolution”. The contrast

changes from dark to light due to the surface layer of Au electrode being reacted and dissolved in the electrolyte. After the surface layer is peeled off, the exposed new surface area of Au electrode reacts with the electrolyte resulting in “second round dissolution”. As shown in Figure 3F-H, the reaction front moves promptly in diagonal direction from 8:10 s to 12.7 s and almost all the Au electrode vanished. Figure 3J shows the corresponding applied electrical potential and measured electrical current from frame A-I, where the applied voltage is ramping from 0 V to -3 V and the measured electrical current decreases. It is noted that the measured electric current is higher under TEM than that from the same electrochemical liquid cell without electron beam and the beam effects will be discussed in a late section. The reaction kinetics is measured by the dissolution area of Au electrode as a function of time. In the first round dissolution, an area of  $4.5 \mu\text{m}^2$  is etched away within 2 s under  $-0.6 \text{ V} \sim -0.8 \text{ V}$ , thus the etching speed of Au electrode is  $2.25 \mu\text{m}^2/\text{s}$ . The Au etching speed of the second round dissolution in the voltage range of  $-0.8 \text{ V} \sim -1.4 \text{ V}$  is  $1.33 \mu\text{m}^2/\text{s}$ . The intensive Au dissolution mostly occurred in voltage range of  $-0.6 \text{ V} \sim -1.4 \text{ V}$ . According to Bach et al,<sup>22</sup> metastable  $\text{AuLi}_2$  can be formed and then dissolved during cyclic voltammetry. We captured the signal of dissolved gold in the surrounding area of the electrode (Figure 5).

Another type of Li-Au reaction that was observed is explosive reaction of the Au electrode. In this case, during lithiation of Au electrode, electrolyte decomposition is still expected but no gaseous products (bubbles) are released. It is likely that the gaseous products are absorbed and accumulated on the surface of electrode, which triggers the explosion of the Au electrode at a later stage. This explosion generates a large number of Au or Li-Au nanoparticles, since Au or lithiated Au can be peeled off from Au electrode

during explosion. In Figure 4A-F, the sequential images show such explosive Au lithiation reaction. Initially, Au electrode is intact with a clean sharp interface with the electrolyte. When the cyclic voltammetry is ramped down in negative direction, inhomogeneous reaction occurred as marked with white dash line in Figure 4C. Subsequently, the splashing of nanoparticles accompanied by erosion of the electrode takes place. The number of splashed particles dramatically increases within 3 s and they reside in the surrounding area of the fragmented electrode.

We did energy dispersive X-ray spectroscopy (EDS) mapping of the reacted Au electrode with the fragmented Au electrode and many small nanoparticles in the surrounding area as well as the other side of the electrode. Figure 5 B and D show the elemental distribution profiles of Au in both reacted and unreacted electrodes. In the reacted Au electrode residual, there is a higher concentration of Au at the edge than the inner part indicating inhomogeneous Li-Au reaction. The front area of Au electrode has a higher intensity of Au, which corresponds to a stronger electric field during reaction. It is clear that the splashed particles from the electrode during Au lithiation contribute to the measured Au signal in the EDS map. It also shows that there is Au in the “clean” area between the particles, suggesting a fraction of Au is dissolved in the electrolyte. On other side of Au electrode, we observe a sharp edge with Au uniformly distributed across the electrode.

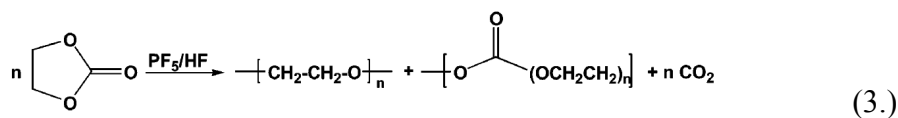
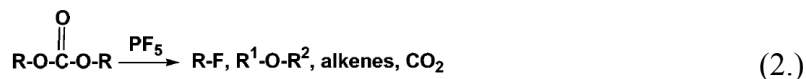
In addition to the above two types of reactions, expansion and shrinkage of Au electrode during discharging and charging are observed. This type of reaction is classical and frequently reported in the literature,<sup>20</sup> which is probably because such reaction can easily be confirmed by ex situ characterization techniques although detailed reaction

dynamic is lacking. Sequential images in Figure 6A-F show the morphology changes of Au electrode during lithiation and delithiation. When voltage is ramped down to -1.7 V, electrolyte bubble started to form (Figure 6A). It is followed by an expansion in the front part of Au electrode (Figure 6B) indicating Au is lithiated. The intensive expansion of electrode induces cracks. The inhomogeneous reaction becomes more and more obvious and some heavy lithiated regions are distributed in the Au electrode. The electrode area with darker contrast represents light lithiation while the brighter contrast indicates heavy lithiation, as marked in blue dash line in Figure 6C. During charge process, shrinkage of the electrode is observed as indicated by the contour changes of the lithiated regions.

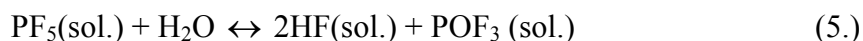
Au is likely catalyzing the electrolyte decomposition during the charge cycles. Obviously, we did see lots of bubbles in Figure 3 in the voltage range of 0 ~ -3 V. There are several factors influencing the electrolyte decomposition including the applied voltage and irradiation of electron beam. Our control experiments suggest the generation of gas bubbles is primarily due to electrolysis of electrolyte. In a previous paper,<sup>23</sup> we discussed the beam effect is secondary to electrolysis in electrolyte decomposition since there is no bubble formation without an electric bias. Here we found that Au may catalyze the electrolysis of electrolyte. This is not surprising since Au is catalytically active in many chemical reactions,<sup>26-29</sup> including those in CO oxidation, Li-O<sub>2</sub> batteries and so forth. Figure 7 A-C (as well as Figure 3) show that the Au electrode is clear with no reactions at the beginning (Figure 7A). When the voltage is ramped down in negative direction, many bubbles appear in the front of the electrode. Small bubbles can accumulate and merge into larger ones up to several micrometers as highlighted in Figure 7B-C. At room temperature, an equilibrium exists:<sup>23, 30</sup>



In the presence of non-aqueous solvents,  $\text{PF}_5$  tends to cause decomposition of carbonates:<sup>30</sup>



It is also known that moisture can induce hydrolysis of  $\text{LiPF}_6$  salts:<sup>30</sup>



In our experiments, we load the electrolyte in glove-box and the moisture effects can be minimized. It is likely that Au is catalyzing the above reactions 1, 2 and 3. For control experiments, we use Ti electrodes to replace Au electrodes. The results show that, when a cyclic voltammetry is applied in the voltage range of 0 ~ -3 V, no severe bubble formation is observed (Figure 7E-F). This supports that Au catalyzing bubble formation from electrolyte decomposition.

The electron beam has strong effect on the current measured from the electrochemical liquid cell under TEM. Previously, we have shown that there is a drastic increase of the current when the cell is exposed to the electron beam.<sup>31</sup> Here, we show the cyclic voltammetry curves measured in an electrochemical cell with/without electron beam. Figure 8A is the CV curve without electron beam passing through. It shows when voltage is ramped down from 0 to -3 V, there is a reduction peak located at -2.1 V corresponding to the lithiation reaction of Au electrode. When the voltage is swept back from -3 V to 0 V, there is an oxidation peak located at -1.45 V, which is attributed to the delithiation

reaction of Au electrode. It is noted that the reduction and oxidation peaks of -2.1 V and -1.45 V are not the exact lithiation/delithiation voltage of Au electrode in lithium ion batteries, since there is no lithium reference electrode in the set up. However, it is clear that the CV plot without electron beam show reduction/oxidation peaks corresponding to lithiation/delithiation of the Au electrode. When the electron beam passes through the electrochemical liquid cell, the CV plot changes drastically with strong current increases (Figure 8B). As the voltage ramps from 0 to -3 V, the current decreases from -63 to -10  $\mu\text{A}$ . Then, when the voltage swept back to positive direction, the current maintains a steady state in -4 ~ -6  $\mu\text{A}$  range while the peak current without electron beam is only 0.77  $\mu\text{A}$ . By comparing these two CV curves, we conclude that in the current experiments the major component of the measured current is from electron beam.

The current changes due to electron beam can be calculated based on TEM imaging condition and electrochemical cell set up. We used an electron current density ( $J$ ) of  $2.5 \times 10^3 \text{ electrons} \cdot \text{\AA}^{-2} \cdot \text{s}^{-1}$  during imaging and the area ( $S$ ) of Au electrodes exposed to electron beam is  $S = 2 L \cdot w$ , where  $L$  is the length ( $L = 10 \mu\text{m}$ ) and  $w$  is the width ( $w = 6 \mu\text{m}$ ) of the Au electrode exposed to electron beam. The current is measured in Amps (charge per second) and  $1 \text{ A} = -6.241 \times 10^{18} \text{ e/s}$ , therefore, the current ( $I$ ) generated from the electron beam can be calculated:  $I = J \cdot S = 2 \cdot J \cdot L \cdot w = -5 \mu\text{A}$ . The calculated value is comparable with the current measured by electrochemical working station under cyclic voltammetry program. This further confirms that the current increase is due to electrons collected directly by the electrodes from electron beam. How such electrons affect the electrochemical reaction including electrolyte decomposition needs to be further studied. The thickness of the Au electrode in the current electrochemical liquid cells is about 120

nm. We expect when the thickness of the electrode is reduced, the current increase from electron beam irradiation can be reduced.

Although the morphology changes of Au electrode during reaction with Li have been observed with great detail as discussed above, it is a great challenge to characterize structure of intermediate Li-Au alloy phases due to the fast reaction kinetics and the amorphous-like reaction products are dissolved at the end. We did parallel ex situ experiments to show the composition and crystal structure of the lithiated Au. As shown in Figure 9,<sup>23</sup> when a single crystal Au nanowire is lithiated both morphology and crystal structure are changed. The electron diffraction pattern confirms the FCC structure of Au crystal (space group  $Fm\bar{3}m$ ) (Inset of Figure 9A). After cyclic voltammetry, the initially straight Au nanowire becomes twisted with meandering morphology (Figure 9B). Using selected area electron diffraction pattern we further identified the phases of Li-Au section, as shown  $Li_{15}Au_4$  phase marked by the red circles (Inset of Figure 9B).<sup>20</sup> The blues circles attribute to the original cubic structure of Au (space group  $Fm\bar{3}m$ ). The atomic resolution of Au and Li ordering in an electrochemical treated Au nanowire reveals that a  $Li_2$  ( $Au_3Li$ ) Li-Au structure in co-existence with the pure Au lattice (111) lattice planes<sup>4, 32</sup> (Figure 9C). From the spatially resolved electron energy loss spectroscopy (EELS) spectra (Figure 9D-E), the Au core with Li-Au alloy shell can be achieved. The Li concentration profile can be extracted by integrating the near edge signal from 56-65 eV as shown in Figure 9E. Au concentration is almost the same with no obvious deviation along the red dash line of the cross section of the Au nanowire. However, the Li concentration is lower in the center of the Au wire, indicating the electrochemical lithiation start from the surface of the Au wire and Li propagates and diffuses towards the

core.<sup>23</sup> Such ex situ study provide some useful information although intermediate phases are missing.

### **Conclusions**

In this paper, we demonstrated in-situ Au lithiation by utilizing electrochemical liquid cell. The observed Li-Au reaction indicating that there are three types morphology changes during Au lithiation: dissolution, explosive reaction and expansion/shrinkage. The possible factors that induced these kinds of Li-Au reactions are discussed. Besides the Li-Au reactions, we also studied bubble formation from electrolyte decomposition and the electron beam effect. The catalytic effects of Au in electrolyte decomposition are observed. More detailed characterization of the intermediate structure during the lithiation of Au is needed by in situ study in future work.

### **Acknowledgments**

We used both MSD TEM facility and TEAM0.5 and CM200 microscopes at National Center for Electron Microscopy (NCEM) of Lawrence Berkeley National Laboratory (LBNL), which is supported by the U.S. Department of Energy (DOE) under Contract # DE-AC02-05CH11231. W.L. is supported by National Science Council in Taiwan under contract number NSC102-2911-I-009-502. H.Z. thanks the support of DOE Office of Science Early Career Research Program. We thank Direct Electron, LP (San Diego, CA) for providing the high speed direct electron camera model DE-12 for movie capture.

## References

1. W. Xu, J. Wang, F. Ding, X. Chen, E. Nasybulin, Y. Zhang and J.-G. Zhang, *Energ. Environ. Sci.*, 2014, **7**, 513-537.
2. M. Gu, Z. Wang, J. G. Connell, D. E. Perea, L. J. Lauhon, F. Gao and C. Wang, *ACS Nano*, 2013, **7**, 6303-6309.
3. J. T. Yin, M. Wada, S. Yoshida, K. Ishihara, S. Tanase and T. Sakai, *J. Electrochem. Soc.*, 2003, **150**, A1129-A1135.
4. Y. J. Lee, Y. Lee, D. Oh, T. Chen, G. Ceder and A. M. Belcher, *Nano Lett.*, 2010, **10**, 2433-2440.
5. H. C. Shin and M. Liu, *Adv. Funct. Mater.*, 2005, **15**, 582-586.
6. W. Luo, S. Lorget, B. Wang, C. Bommier and X. L. Ji, *Chem. Commun.*, 2014, **50**, 5435-5437.
7. Z. Y. Zeng, J. P. Tu, Y. Z. Yang, J. Y. Xiang, X. H. Huang, F. Mao and M. Ma, *Electrochim. Acta*, 2008, **53**, 2724-2728.
8. Z. Y. Zeng, J. P. Tu, X. L. Wang and X. B. Zhao, *J. Electroanal. Chem.*, 2008, **616**, 7-13.
9. Z. Y. Zeng, J. P. Tu, X. H. Huang, X. L. Wang, X. B. Zhao and K. F. Li, *Electrochem. Solid St. Lett.*, 2008, **11**, A105-A107.
10. Z. Y. Zeng, J. P. Tu, X. H. Huang, X. L. Wang and J. Y. Xiang, *Thin Solid Films*, 2009, **517**, 4767-4771.
11. G. Taillades, N. Benjelloun, J. Sarradin and M. Ribes, *Solid State Ionics*, 2002, **152**, 119-124.
12. H. Zheng, R. K. Smith, Y.-w. Jun, C. Kisielowski, U. Dahmen and A. P. Alivisatos, *Science*, 2009, **324**, 1309-1312.
13. H.-G. Liao, L. Cui, S. Whitlam and H. Zheng, *Science*, 2012, **336**, 1011-1014.
14. K. W. Noh and S. J. Dillon, *Scripta Mater.*, 2013, **69**, 658-661.
15. M. Gu, L. R. Parent, B. L. Mehdi, R. R. Unocic, M. T. McDowell, R. L. Sacci, W. Xu, J. G. Connell, P. Xu, P. Abellan, X. Chen, Y. Zhang, D. E. Perea, J. E. Evans, L. J. Lauhon, J.-G. Zhang, J. Liu, N. D. Browning, Y. Cui, I. Arslan and C.-M. Wang, *Nano Lett.*, 2013, **13**, 6106-6112.
16. M. E. Holtz, Y. Yu, D. Gunceler, J. Gao, R. Sundararaman, K. A. Schwarz, T. A. Arias, H. D. Abruña and D. A. Muller, *Nano Lett.*, 2014, **14**, 1453-1459.
17. P. Abellan, B. L. Mehdi, L. R. Parent, M. Gu, C. Park, W. Xu, Y. Zhang, I. Arslan, J.-G. Zhang, C.-M. Wang, J. E. Evans and N. D. Browning, *Nano Lett.*, 2014, **14**, 1293-1299.
18. R. L. Sacci, N. J. Dudney, K. L. More, L. R. Parent, I. Arslan, N. D. Browning and R. R. Unocic, *Chem. Commun.*, 2014, **50**, 2104-2107.
19. C.-M. Wang, X. Li, Z. Wang, W. Xu, J. Liu, F. Gao, L. Kovarik, J.-G. Zhang, J. Howe, D. J. Burton, Z. Liu, X. Xiao, S. Thevuthasan and D. R. Baer, *Nano Lett.*, 2012, **12**, 1624-1632.
20. L. Yuan, H. K. Liu, A. Maarroof, K. Konstantinov, J. Liu and M. Cortie, *J. New Mater. Electr. Sys.*, 2007, **10**, 95-99.
21. B. Laik, L. Eude, J. P. Pereira-Ramos, C. S. Cojocaru, D. Pribat and E. Rouviere, *Electrochim. Acta*, 2008, **53**, 5528-5532.

22. P. Bach, A. Seemayer, U. Ruett, O. Gutowski and F. Renner, *DESY Photon Science Annual Reports*, 2012.
23. Z. Y. Zeng, W. I. Liang, H. G. Liao, H. L. L. Xin, Y. H. Chu and H. M. Zheng, *Nano Lett.*, 2014, **14**, 1745-1750.
24. A. D. Pelton, *Bulletin of Alloy Phase Diagrams*, 1986, **7**, 228-231.
25. P. Limthongkul, Y. I. Jang, N. J. Dudney and Y. M. Chiang, *Acta Mater.*, 2003, **51**, 1103-1113.
26. B. Hvolbæk, T. V. W. Janssens, B. S. Clausen, H. Falsig, C. H. Christensen and J. K. Nørskov, *Nano Today*, 2007, **2**, 14-18.
27. T. V. W. Janssens, A. Carlsson, A. Puig-Molina and B. S. Clausen, *J. Catal.*, 2006, **240**, 108-113.
28. S. H. Overbury, V. Schwartz, D. R. Mullins, W. Yan and S. Dai, *J. Catal.*, 2006, **241**, 56-65.
29. Z. Peng, S. A. Freunberger, Y. Chen and P. G. Bruce, *Science*, 2012, **337**, 563-566.
30. K. Xu, *Chem. Rev.*, 2004, **104**, 4303-4417.
31. M. Sun, H.-G. Liao, K. Niu and H. Zheng, *Sci. Rep.*, 2013, **3**, 3227.
32. H. L. Xin, J. A. Mundy, Z. Y. Liu, R. Cabezas, R. Hovden, L. F. Kourkoutis, J. L. Zhang, N. P. Subramanian, R. Makharia, F. T. Wagner and D. A. Muller, *Nano Lett.*, 2012, **12**, 490-497.

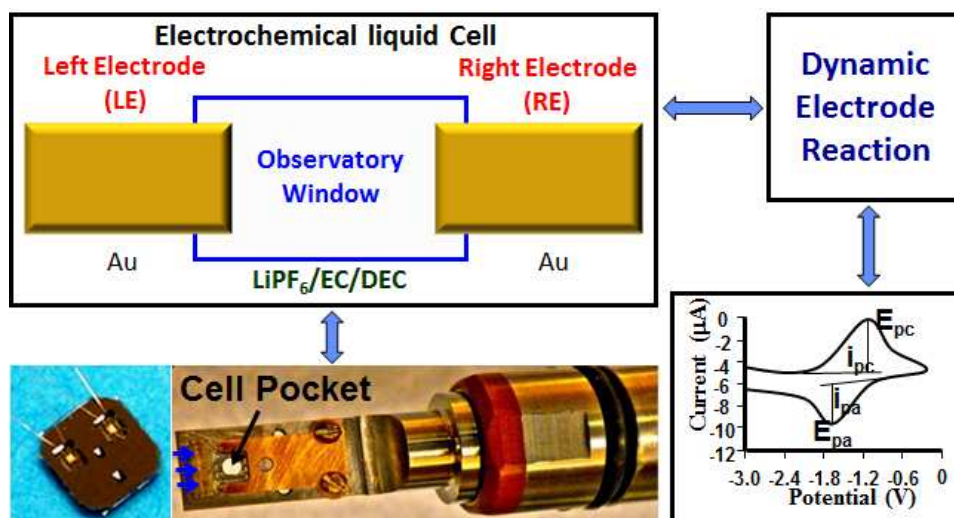


**Figure 1.** A scheme of in situ TEM set up for the observation of electrochemical reaction using an electrochemical liquid cell. 120 nm thick gold (or Ti) electrodes are used. The dynamic electrochemical reaction on the electrode corresponding to the applied cyclic voltammetry is captured. Bottom left photographs are an electrochemical liquid cell and a home-made TEM holder.

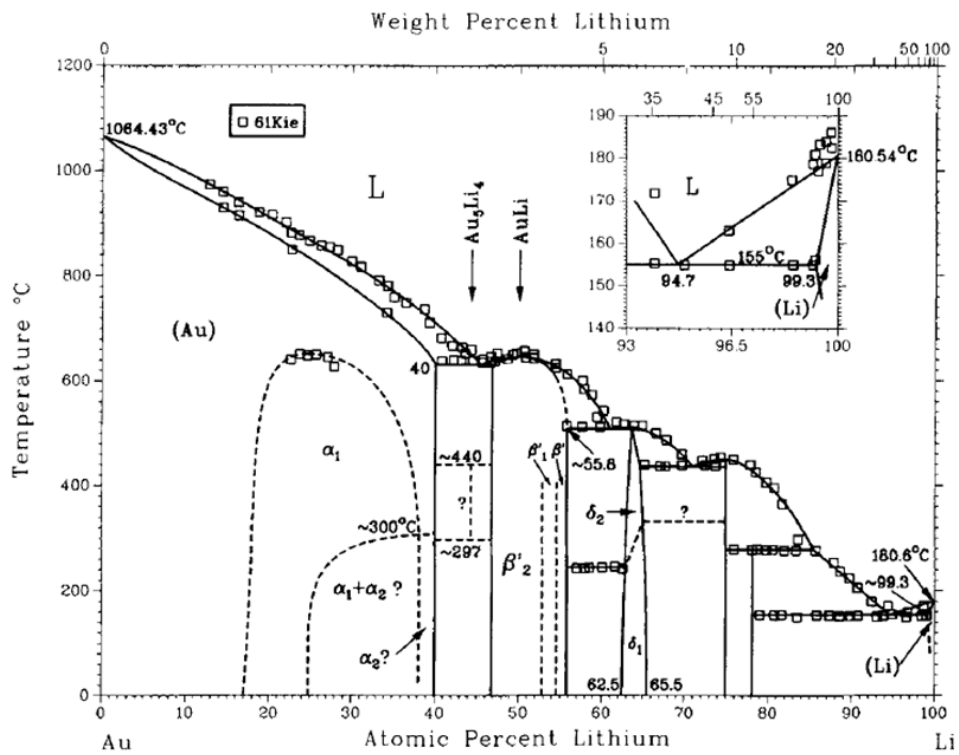
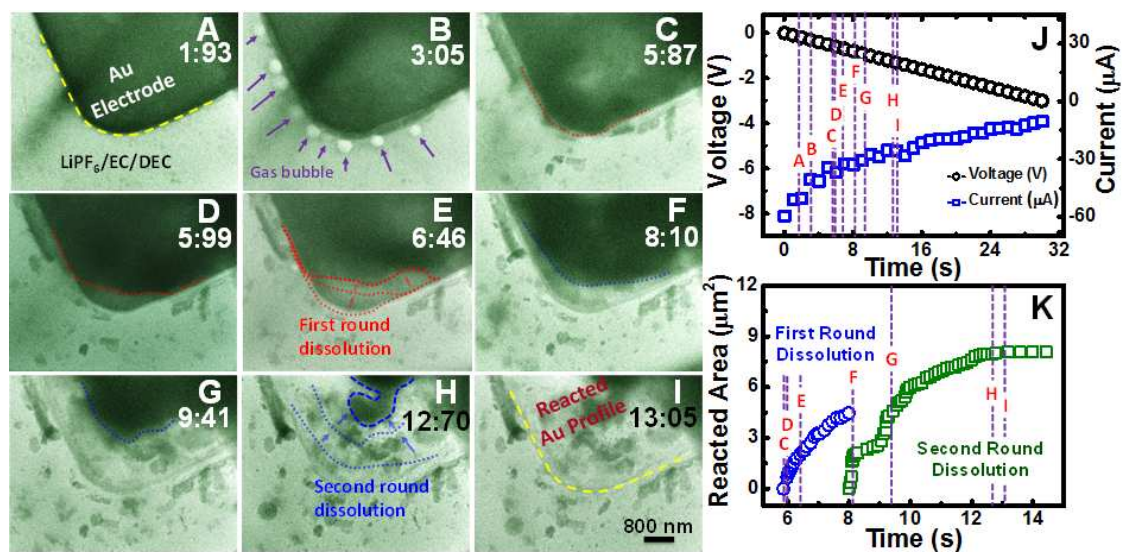
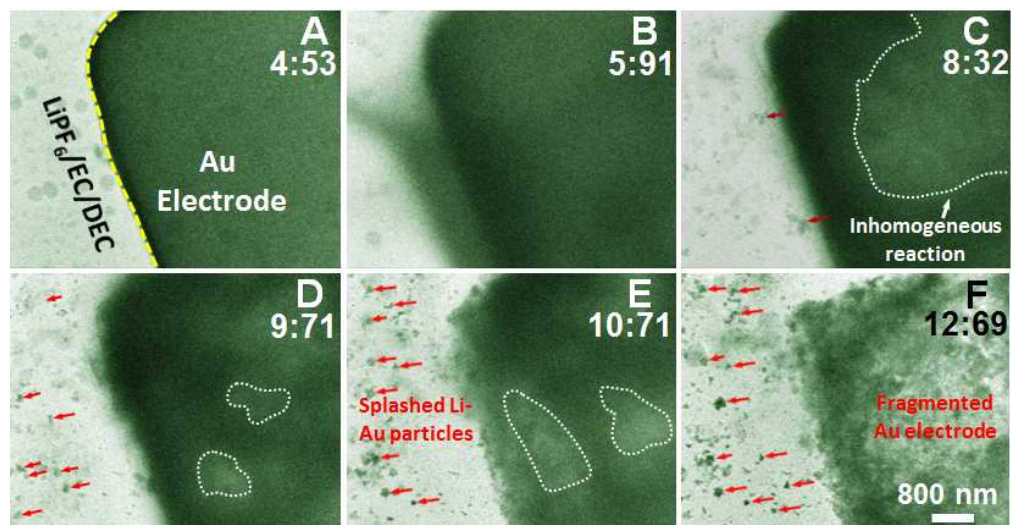


Figure 2. Au-Li Phase Diagram.<sup>22</sup>



**Figure 3.** (A-I) Time evolution of the dissolution of Au electrode in LiPF<sub>6</sub>/EC/DEC electrolyte; (J) The corresponding applied electric potential and measured electric current from frame A to frame I; (K) The evolution of the dissolved area in Au electrode as a function of time during cyclic voltammetry with the voltage range 0 ~ -3 V and scan rate of 0.1 V/s.



**Figure 4.** Time series of TEM images showing the inhomogeneous and fragmentation of Au electrode during Li-Au reaction. During this explosive reaction, a large number of nanoparticles splashed from Au electrode to the surrounding area of the electrode.

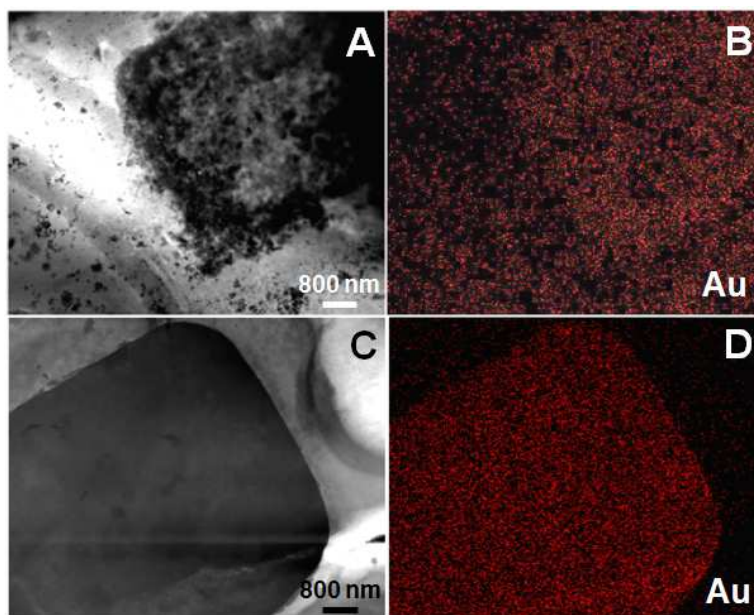


**Figure 5.** (A) TEM image of the right Au electrode that was electrochemically reacted with lithium electrolyte (also shown in Figure 4F). (B) The corresponding EDS map of B. (C) The Left side of Au electrode. (D) The corresponding EDS map of Au electrode in C.

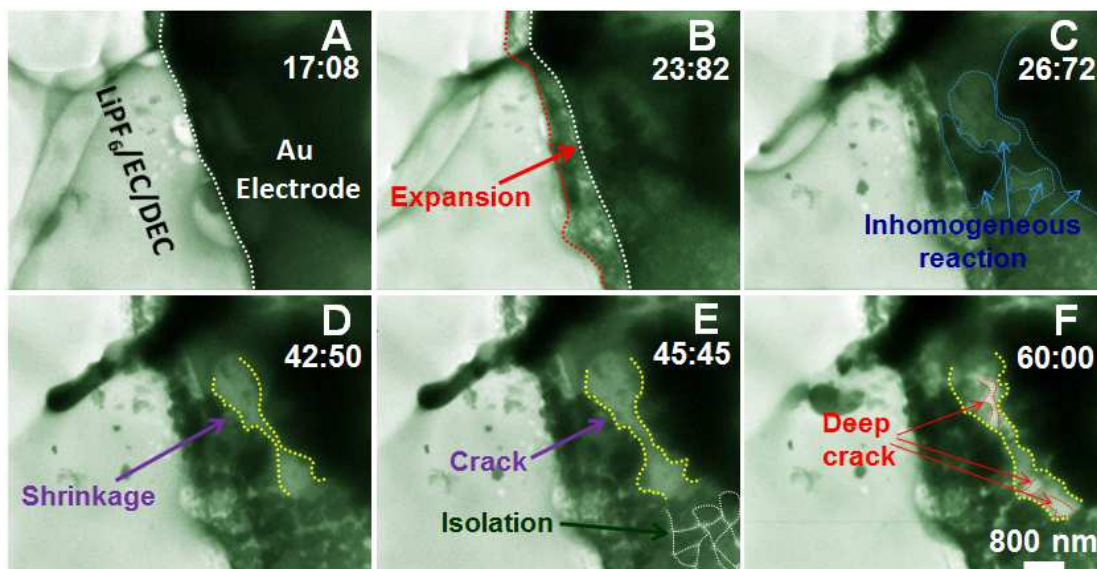


**Figure 6.** Evolution of Au electrode when electrochemically reacted with lithium electrolyte. Expansion, cracking and partial shrinkage are observed.

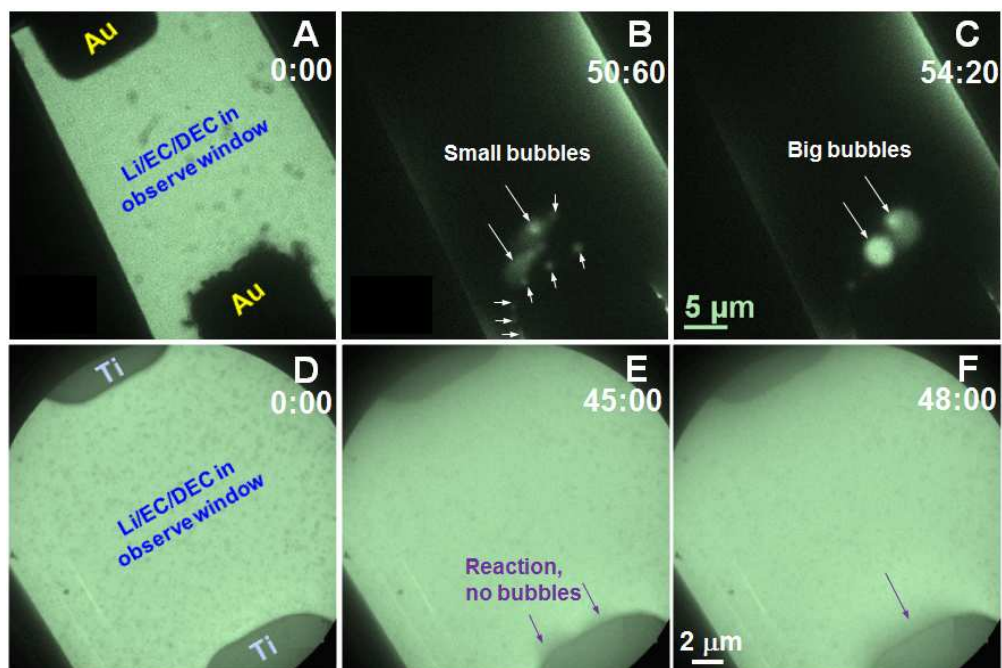


**Figure 7.** Sequential images show electrode-electrolyte interface reaction on both side of electrodes in two electrochemical cells. Au electrodes are used in (A-C) and Ti electrodes are used in (D-F).

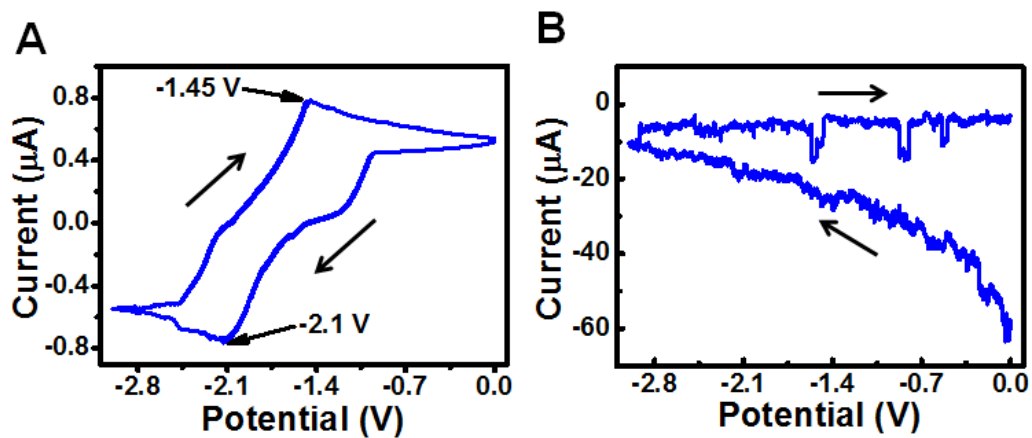


**Figure 8.** Cyclic voltammetry without (A) or with (B) electron beam passing through the SiNx membrane in the same electrochemical liquid cell.

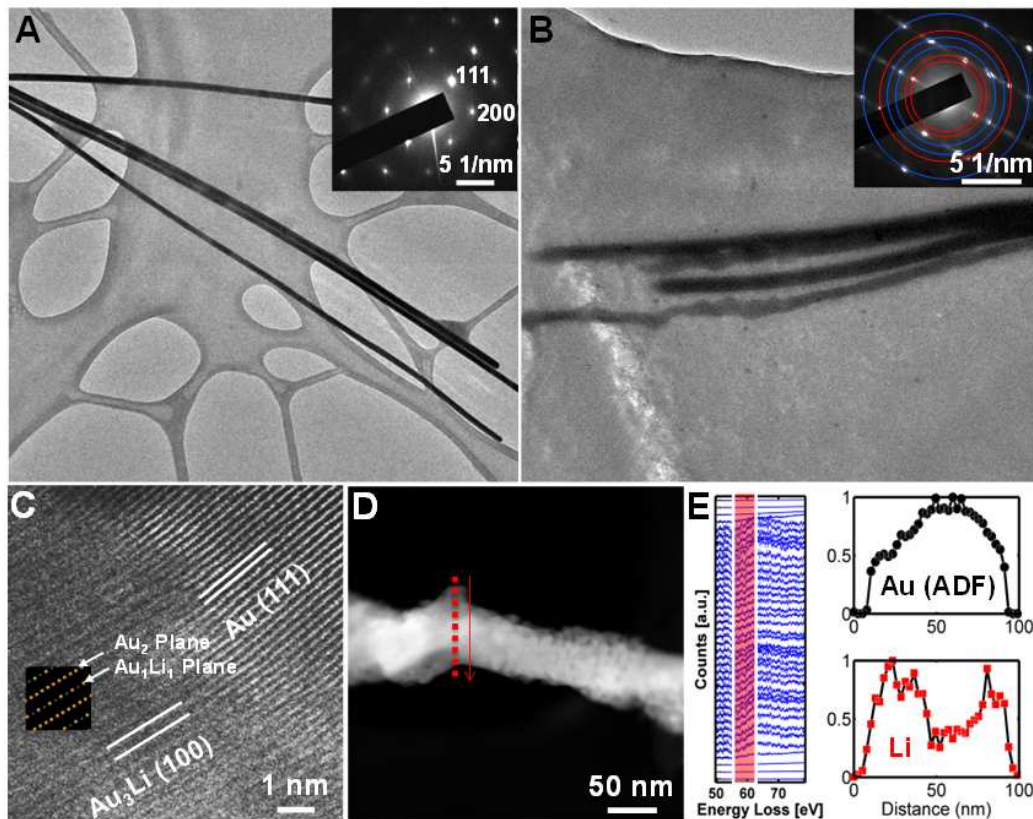


**Figure 9.** Ex-situ TEM studies of gold nanowires before and after the charge cycles. (A) TEM image of gold nanowires before lithiation and the corresponding Selected Area Electron Diffraction Pattern (SAED; inset). (B) TEM image of lithiated Au nanowires and the corresponding SAED (inset). (C) High resolution TEM image of lithiated Au nanowire with  $\text{Au}_3\text{Li}$  structure. The alternating planes of  $\text{Au}_2$  and  $\text{Au}_1\text{Li}_1$  are shown in the model structure (Au in yellow; Li in Blue). (D) HAADF image of a lithiated Au nanowire. The electron energy loss spectroscopic (EELS) line profile is along the dash line. (E) Extracted lithium and gold concentration along the line profile in D with the maximum intensity was normalized to 1. Lithium concentration was integrated from the Li K-edge (56-65 eV) (Au O edge contribution in the energy range is negligible. Gold concentration was estimated from the ADF signals).<sup>23</sup>